EasyChair Preprint

№ 13283

Modelling, Parametrizing and Simulating a DEM-Based Soil-Model for Industrial Applications

Sebastian Emmerich, Georg Franosch, Michael Burger, Anita Ullrich and Johannes Quist

May 14, 2024

The 7th International Conference on Multibody System Dynamics
June 9-13, 2023, Madison, WI, USA

Modelling, Parametrizing and Simulating a DEM-Based Soil-Model for Industrial Applications

Sebastian Emmerich*, Georg Franosch*, Michael Burger*, Anita Ullrich†, Johannes Quist†

* Department of Dynamics, Loads and Environmental Data
Division Mathematics for Vehicle Engineering
Fraunhofer Institute for Industrial Mathematics
Fraunhofer-Platz 1, 67663 Kaiserslautern, Germany
[sebastian.emmerich, georg.franosch, michael.burger]@itwm.fraunhofer.de

† Department of Computational Engineering and Design
Fraunhofer-Chalmers Centre for Industrial Mathematics
Chalmers Science Park, 41288 Gothenburg, Sweden
[anita.ullrich, johannes.quist]@fcc.chalmers.se

ABSTRACT

Simulation and simulation-assisted methods have a large impact for product development in many industrial fields. Multibody dynamics (MBD) simulation, for instance, is an established method used for durability analysis and energy efficiency calculations in vehicle engineering, based on its ability to provide accurate prediction of interaction forces. In the domain of off-road vehicles and heavy machinery, such considerations need to be expanded by a method to model the soil and its interaction with the vehicle, i.e., the soil-tool interaction, as the resulting forces may drastically influence the durability and energy efficiency of the machine. Therefore, the model must be chosen carefully to maintain the high accuracy in the force prediction for the soil-tool interaction, as required for a reliable and robust product development.

In this contribution, we present a workflow to tackle this topic, based on a co-simulation scheme between an MBD-based vehicle model and a particle simulation realized in the Discrete Element Method (DEM). The simulated soil is parametrized and validated by matching simulation results from a virtual experiment with measurement data from real-world soil laboratory experiments as the triaxial compression test. Using this process, the applicability and performance of the numerical methods can be determined.

1 INTRODUCTION

Accurate force prediction and decent model fidelity are key ingredients in the field of simulation-assisted vehicle development, enabling the engineer to access durability properties or energy consumption quantities without the need of hardware prototyping. The immediate accessibility of model parameters and variables within the simulation environment and the permanent availability of the prototype's digital twin facilitate faster testing and development iteration loops. While, for on-road vehicles, modelling the vehicle and its operator is sufficient for most applications, for off-road vehicles and heavy machinery, the interaction of their tool with a granular soil material is crucial for the development process. Consequently, the employed simulation framework needs to be extended by a method to predict the force feedback generated by a granular material. While there are multiple approaches for the simulation of granular materials, based on continuum methods as the Finite Element Method or Smoothed Particle Hydrodynamics [1], most of the published implementations are based on the Discrete Element Method (DEM) [2]. DEM has first been applied to rock mechanics by Cundall and Strack in 1979 [3] and has shown great potential for the accurate prediction of soil-tool interaction forces [4, 5, 6].

For the purpose of this work, the DEM solver "Demify® for Heavy Machinery and Vehicles" (Demify® HMV) has been employed. It results from a long-lasting cooperation between the Fraunhofer ITWM and the Fraunhofer-Chalmers Centre (FCC) [10]. The solver yields highly accurate predictions for draft forces and soil-tool interaction, e.g., coarse sand and natural soils using spherical particles and coarse-graining methods [8], and produced rock material products using a complex shape solver.

To ensure a match to the real world, a validation procedure has been established [8, 12]. Figure 1 illustrates the proposed workflow for a validated draft force prediction in simulation, usable for different industrial applications. Validation of the simulated soil with experimental tests ensures the realistic soil behavior for later application. In this context, the parametrization of the simulated soil is optimized by matching the results from a triaxial test simulation to real-world triaxial test data (see Section 3). This validation guarantees the correct force prediction during the actual simulation scenario, where the soil is interacting with the tool and the machine in a co-simulation setup (see Section 4). Load data acquired in this simulation can then be used for durability and fatigue analysis or for energy efficiency studies in development processes, e.g., for new machine generations [7].

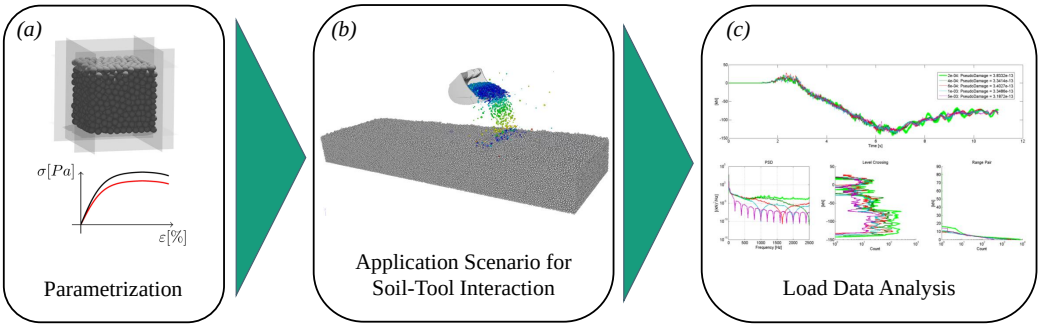

Figure 1. Steps of workflow: The soil sample is parametrized via simulation of a real-word experiment *(a)*. This soil is used in an MBD-DEM co-simulation scheme to predict soil-tool interaction forces *(b)*. The resulting load data is acquired and analyzed *(c)*.

In Section 3, the parametrization and validation process for the soil model will be examined and discussed in more detail, since it is the important and crucial first step of the workflow. The resulting soil sample is then used in an exemplary application scenario to predict soil-tool interaction forces in a co-simulation framework. For this purpose, a digging maneuver performed by a wheeled excavator has been chosen.

2 METHODOLOGY

The granular soil is simulated as a particle system with Fraunhofer's DEM solver Demify®, a GPU-based high performance computing software facilitating efficient collision detection with a bounding volume hierarchy (BVH) [16]. The solver has a Python advanced programming interface (API), which enables the co-simulation with MBD-DEM via a functional mockup interface (FMI) [15]. Simulation cases set up with Demify® can be packaged as a functional mockup unit (FMU) using the package PyFMU [20]. The details of the DEM implementation are omitted for brevity, the interested reader is referred to the given references.

Demify® is capable of simulating different industrial problems and scales and is applied for e.g. roller compaction with Demify HMV [17], railroad simulations [19] and additive manufacturing [18]. The parallelization on the GPU allows for the simulation of millions of particles and the BVH collision detection facilitates efficient collision detection even in large spatial domains enabling the simulation of complete industrial systems.

The MBD simulations are performed with Matlab Simulink, where the FMU can be imported, enabling the DEM-MBD co-simulation with Demify HMV.

In this paper, the granular soil is modelled with sphere particles and rigid objects, such as the walls in the triaxial test, are represented by triangle meshes. Both, the particle-particle interaction and the interaction between particles and rigid objects is based on a linear-spring model [8]. This linear-spring model is based on a normal and a tangential spring-damper element and a tangential friction, parametrized via the parameters

- normal and tangential stiffness E_n and E_t, i.e., (Young's modulus),
- the normal and tangential relative damping coefficient ν_n and ν_t and
- the tangential friction coefficient μ.

In the next Section, the optimization process for finding and validating a virtual soil sample based on these parameters, is described.

3 SOIL CHARACTERIZATION

In order to employ a DEM-based particle simulation in the context of robust and reliable draft force prediction, a precise model calibration and validation procedure is required. Here, we use a calibration technique based on the reproduction of experimental soil laboratory data in a virtual version of the same experiment. The experimental data has been acquired using a sample of the real soil that needs to be virtualized.

In Section 3.1, the real world experiment is described and the relevant material and interaction parameters are mentioned. In Section 3.2, the virtual experiment, which is based on the methodology introduced in Section 2, is described in more detail. Furthermore, in Section 3.3, the workflow of adjusting the parameters is explained. The resulting parameters are presented in Section 3.5.

3.1 Experimental soil characterization

The parameter set required for a virtual soil sample contains several quantities, some of which can be direclty accessed in dedicaded experiments. These quantities contain material characteristics as the grain size distribution, the porosity Φ and the density ρ of the grain material which are determined using standard setups as, e.g., sieving tests for the determination of the grain size distribution.

Moreover, there are material properties which need to be accessed indirectly, as the internal friction angle ϕ, which is typically determined via the measurement of several strain-stress curves.

While there are different standardized tests to access the stress-strain properties of the soil sample, e.g. direct shear or linear penetration tests, studies carried out in [12] revealed the triaxial test as the best suiting for the further workflow. Especially in the comparison between real and virtual experiment, needed for the parametrization routine of the virtual soil sample, the triaxial test shows consistent and robust behavior, as will be discussed later.

For this test, a soil sample is filled into a rubber tube. This tube is surrounded by water which exerts a constant pressure Δp on the soil sample, as can be seen in Figure 2*(a)*. Once the soil reaches a static condition, a piston starts slowly pushing the sample from the top, thus compressing the soil while acting against the water pressure. The force applied to the piston is recorded alongside the quasi linearly increasing strain [13]. The emerging stress-strain curve of the real world soil sample is used to find and validate the parametrization of the virtual soil sample, as shown in Section 3.2.

The reason for this iterative approach is the limited accessibility of parameters. So, the internal friction angle ϕ can't be directly set into the particle code, while interaction parameters as Young's modulus E, the relative damping ν or the tangential friction coefficient μ can't be accessed experimentally.

3.2 Virtual experiment

Before the triaxial test can be executed, similar to the real-world experiment, the virtual soil sample needs to be prepared. For this purpose, in this sample generation phase, particles are created and dropped into a box with the same size as the triaxial test box. The sizes of the particles are chosen according to a normal distribution with its mean value at the average particle size and a maximum and minimum particle size as well as a given standard deviation. These values are obtained by checking the results of the sieving test. The amount of particles generated is dependent on the given mass flow q_m. The theoretical mass m of all

needed particles can be calculated with

$$m = \rho(1 - \Phi)V \tag{1}$$

with volume of the triaxial test V, density ρ and porosity Φ. The sample is generated over $\Delta t = 9s$ so the theoretical mass flow should be

$$q_m = \frac{\Delta m}{\Delta t}. \tag{2}$$

As the porosity of the generated particle pile is lower than in the experiment, a greater mass flow is needed to fill the box completely. Particles exceeding the box are removed in the last time steps of the sample generation.

In the triaxial test phase, the generated sample is compressed. As mentioned in [10], the cylindrical box of the experiment can be approximated by a square box. The resulting setup can be seen in Figure 2*(a)*. The pressure Δp, exerted by the surrounding water, is mirrored in the simulation by moving the box walls perpendicular to the piston, i.e., the four walls' positions are changed in a control loop, resulting in a constant sidewall pressure. The pressure exerted by the sample against the piston is recorded and compared to the stress-strain curve of the real-world experiment.

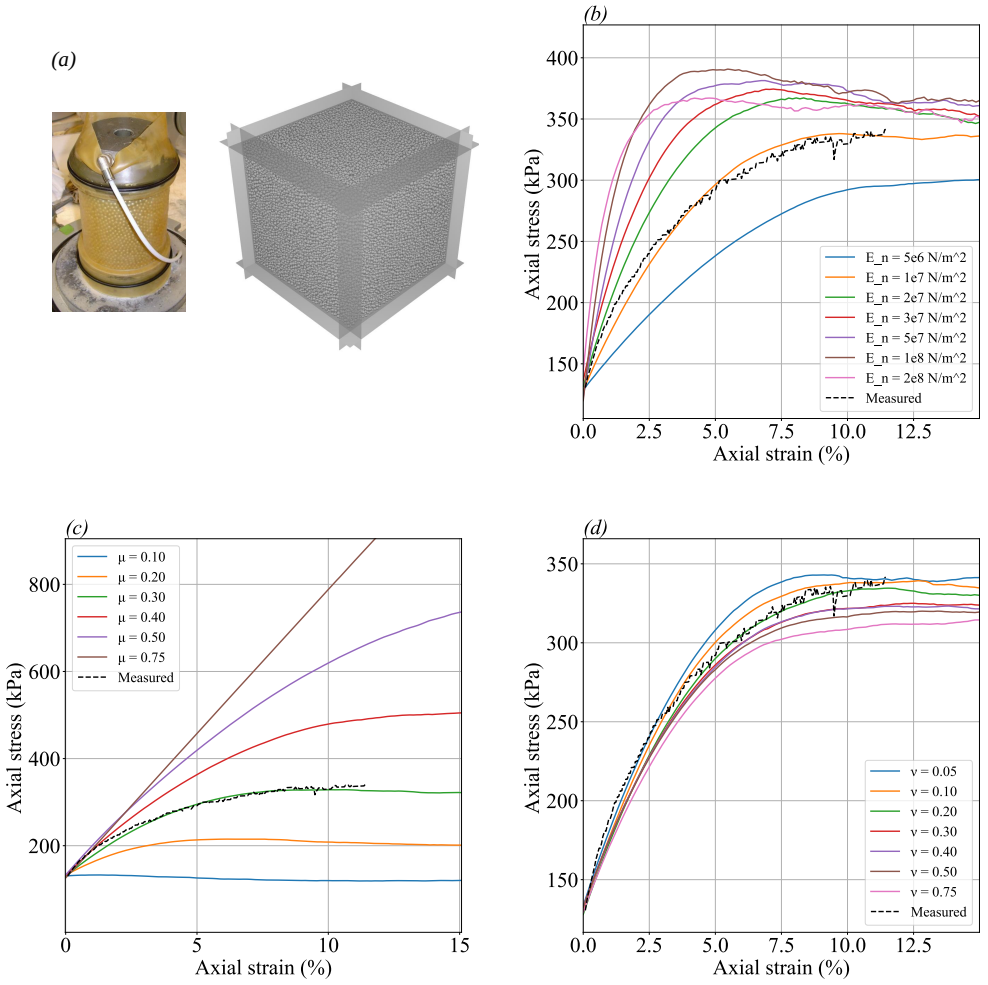

Figure 2. Visual representation of virtual and real triaxial test setup *(a)* and variation of the interaction parameters: Young's modulus *(b)*, friction coefficient *(c)* and relative damping parameter *(d)*.

3.3 Workflow

In order to achieve a set of parameters for the virtual soil with similar stress-strain behavior as the real soil, the stress-strain curves of the real-world and the virtual triaxial tests are compared. The influence of different parametrizations on the stress-strain behavior has been examined in several parameter variation studies. Exemplary curves of these studies are shown in Figure 2. These studies are used to get an understanding of each individual parameter's influence on the stress-strain behavior. Based on the observations of these studies, the next sets of parameters can be chosen in order to achieve convergence in an iterative process. For the study, a gravel sand sample with a grain size distribution with a mean particle size of $\mu = 0.040\,\mathrm{m}$, a standard deviation of $\sigma = 0.012\,\mathrm{m}$ and minimum and maximum particle size of $d_{\mathrm{min}} = 0.016\,\mathrm{m}$ and $d_{\mathrm{max}} = 0.063\,\mathrm{m}$ has been employed.

- **Variation of Young's Modulus:** Young's modulus, or, the soil stiffness E, is represented by the tangential stiffness E_{t} and the normal stiffness E_{n} within the virtual soil parameter set. Using a rule of thumb, here, we assume they are linearly dependent [9]. Figure 2*(b)* shows a parameter variation study. For the linear regime of the stress-strain curve, a higher Young's modulus leads to a steeper slope. Also, a higher value of Young's modulus leads to a higher saturation value and a more pronounced maximal stress before soil failure. The behavior in the linear regime is rather intuitive, as it corresponds to the behavior observed in tensile tests.
- **Variation of Friction Coefficient:** The friction coefficient enables a force interaction, when two particles move in tangential direction. In Figure 2*(c)*, it is varied from 0.1 to 0.75. Varying this parameter mainly changes the saturation at the right part of the curve. Consequently, a higher friction is causing higher saturation stress. Similarly to Young's modulus, increasing friction also leads to a steeper slope for the stress-strain curve in the linear regime, but on a much lower scale.

  By increasing or decreasing the friction coefficient and contrarily decreasing or increasing Young's modulus, both parts of the simulated curve are fitted to match the measured curve as well as possible.
- **Variation of damping parameter:** The damping parameter doesn't have as big of an impact as the previous two parameters. As shown in Figure 2*(d)*, increasing the damping parameter lowers the whole curve; the increase in the first part of the curve is less steep and the saturation is on a lower level, however on a much smaller scale than with the other parameters. That's why, in line with previous studies [10], the damping parameter is kept on the same level for the parameter variation.

3.4 Examination of the influence of Coarse-Graining

As has been shown e.g. in [12], the particle interaction model employed here is scale-invariant, enabling the use of larger particles without impacting the resulting interaction forces. To describe this change in particle size, the coarse-graining factor CG is introduced. This coarse-graining factor is defined to describe the increase of particle parameters, e.g., a coarse-graining factor $\mathrm{CG} = 2$ doubles the particles radii, while still maintaining the relative grain size distribution as determined experimentally in Section 3.1.

With a constant cumulative mass or volume of the sample, coarse-graining results in a great reduction of the the number of particles, e.g., $\mathrm{CG} = 2$ would result in a particle number being reduced by a factor of 8. Consequently, the technique is used to optimize computing performance, as it enables to calculate the similar macroscopic forces with less microscopic interaction pairs to be evaluated. While this benefit doesn't play out when using highly parallelized GPU solvers, it still enables to use a larger particle bed. Figure 3 shows the influence of coarse-graining to the stress-strain curves obtained in virtual triaxal tests, ranging up to coarse-graining factors of $\mathrm{CG} = 10$. Figures 3*(a),(b)* show a very similar behavior for low factors, with factors much higher than $\mathrm{CG} = 3$ resulting in unwanted deviations of the strain-stress behavior. Still, a coarse-graining factor of $\mathrm{CG} = 3$ reduces the number of particles by more than 96% without compromising too much accuracy.

It has to be stated that the absolute value of the coarse-graining factor, even if being the observable in this study, is not the critical variable. The actual variable of interest is the ratio between the mean coarse-grained particle diameter $\mu_{\mathrm{CG}} = \mathrm{CG} \cdot \mu$ and the distance between rigid objects as walls or tools Δd_{obj} [21]. For the present study, this translates to an observation, as depicted in Figures 3*(c),(d)*: For $10\mu_{\mathrm{CG}} > \Delta d_{\mathrm{obj}}$,

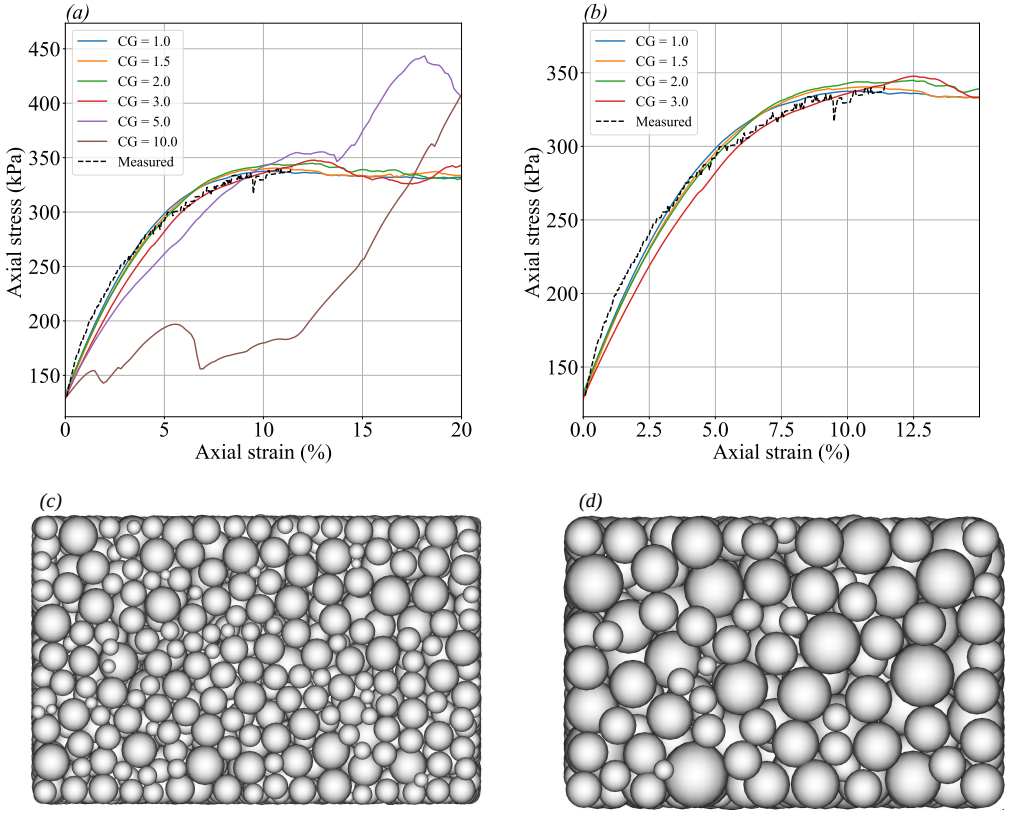

Figure 3. Variation of coarse-graining factor with values of CG up to 10 *(a)* and up to 3 *(b)*, vertical cuts through the triaxial test cell for CG $= 5$ *(c)* and CG $= 3$ *(d)*.

corresponding to a value of the coarse-graining factor CG > 3 for the shown triaxial box, the number of particles between two rigid objects is not large enough to average out the stresses exerted by the sample well enough to yield plausible results.

3.5 Parameter Set of Calibrated Virtual Soil Sample

Summing up the characterization process, the parameter variation studies resulted in a final set of parameters, which will be used to predict soil-tool interaction forces via an DEM-MBD co-simulation scheme in Section 4.

Following the experimental sieving curve, the grain size distribution has been set to a mean particle size $\mu = 0.040\,\text{m}$ with a standard deviation of $\sigma = 0.012\,\text{m}$ and minimum and maximum particle sizes of $d_{\text{min}} = 0.016\,\text{m}$ and $d_{\text{max}} = 0.063\,\text{m}$. In total, the real-world triaxial test has been executed for three sidewall pressures $\Delta p = \{35, 60, 85\}\,\text{kPa}$. Consequently, the virtual triaxial test has also been performed with these three pressures applied. For the parameter variation study, the medium sidewall pressure of $\Delta p = 60\,\text{kPa}$ has been used. Here, simulations of the two sidewall pressures which have not been used for the calibration routine are used as validation of the found parameter set.

Table 1. Final set of interaction parameters resulting from calibration routine.

Soil Type	$E_n(\text{N/m}^2)$	$E_t(\text{N/m}^2)$	ν_n	ν_t	μ
Gravel Sand	$1.125 \cdot 10^7$	$1.35 \cdot 10^7$	0.1	0.1	0.305

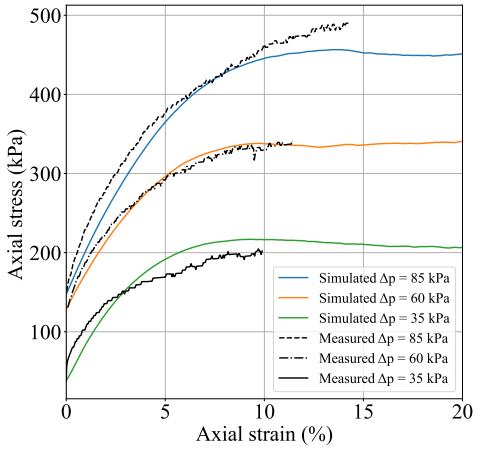

Figure 4. Stress-strain curve for the parameters used for the digital twin of the soil sample.

The final interaction parameters have been summarized in Table 1. The resulting stress-strain curves, showing only small deviations between experimental and virtual soil behavior for all three sidewall pressures, are shown in Figure 4.

4 SIMULATION OF SOIL-TOOL INTERACTION

The digital twin of the real soil sample created in Section 3 has then been applied to the vehicle development in a DEM-MBD co-simulation scheme, yielding the accurate prediction of soil-tool interaction forces, as needed for durability or energy efficiency calculations. To evaluate relevant variables like forces at critical linkage joints of construction machines, e.g., excavator arm joints, a co-simulation in MATLAB/Simulink [14] is used for the purposes of this paper. A Functional Mock-up Interface (FMI) [15] enables this coupling of multibody system and Demify HMV.

4.1 Co-Simulation Setup

The data transfer between the DEM-based particle solver and the MBD solver is established via a parallel Jacobi co-simulation scheme [7]. The tool representation within the DEM solver is moved via displacement information from the current tool position within the MBD simulation, receiving back the current interaction force acting between soil and the tool.

As typical step sizes for the particle solver are in the range of $\Delta t_{\mathrm{DEM}} = 10^{-5}$ s to $\Delta t_{\mathrm{DEM}} = 10^{-4}$ s, while the MBD solver step size is typically about $\Delta t_{\mathrm{MBD}} = 10^{-3}$ s, between synchronization time steps, the MBD solver needs to extrapolate the input values received from the MBD solver. To enhance the extrapolation quality, the MBD solver transmits the tool velocity $\dot{\boldsymbol{x}}$ together with the tool displacement $\boldsymbol{x}$, resulting in a linear tool motion between the synchronization time steps.

In the following, the co-simulation of a digging maneuver, performed by a wheeled excavator model, is used to illustrate the workflow.

4.1.1 MBD Simulation Model

The MBD model's motion, defining the tool path during the co-simulation, can be controlled in different ways, spanning from the replay of a recorded motion to employing a dedicated operator model. If an operator model together with the full MBD model is to be used, the operator model sets the inputs for

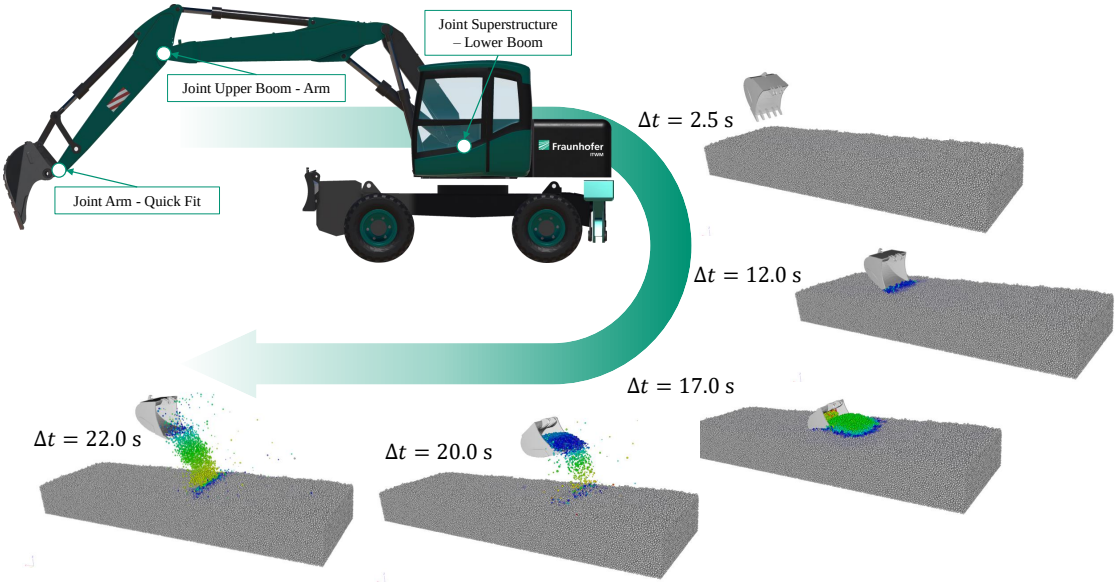

Figure 5. Exemplary application scenario: Snapshots of the particle bed during the digging maneuver, executed by a wheeled excavator. The top left view shows a rendered version of the employed MBD model. The particles' color code depicts their velocity norm. The joints relevant for the constraint force measurements are marked.

a hydraulics model coupled to the movable parts. This approach is especially useful for the design of components, e.g., within the hydraulics system, as required pressures and cylinder dimensions are part of the simulation environment. However, the trajectory will change depending on the capabilities of the hydraulics parametrization and the soil properties. A second approach is the recording of the maneuver in a pre-processing step, including the motion of all moveable parts of the excavator, either using a real machine or its digital twin in interactive simulation. Here, the recording of the tool motion trough the air is used as input for a reduced MBD model, which is coupled to the DEM solver. The hydraulics is neglected for the MBD-DEM co-simulation, but the tool trajectory through the soil is better maintained.

For the present case, the second option has been chosen, i.e., the machine's maneuver has been recorded previously in interactive simulation, taking advantage of a Simulink-based MBD wheeled excavator model at hand. The model includes a real-time capable hydraulics simulation, enabling the operator to control the MBD model's motion during runtime. The tool trajectory has been recorded with no soil-tool interaction enabled, resulting in a steady and smooth movement. The recording contains the motion data of all movable parts of the excavator model, needed as inputs for the reduced MBD model coupled to the DEM solver. The reduced model still includes a tire-soil contact model, ensuring a realistic machine behavior in cases like, e.g., loosing contact with the ground in case of high soil-tool interaction forces.

4.1.2 DEM Particle Testbed

The DEM testbed has been generated within rigid body box with inner diameters of $(10.00 \times 3.00 \times 1.25)\,\mathrm{m}^3$ (length $\times$ width $\times$ height), using the parameters found in Section 3:

The parameters for the *particle-particle interaction* have been set to $E_\mathrm{n} = 1.125 \cdot 10^7\,\frac{\mathrm{N}}{\mathrm{m}^2}$ and $E_\mathrm{t} = 1.35 \cdot 10^7\,\frac{\mathrm{N}}{\mathrm{m}^2}$ normal and tangential stiffness, $\nu_\mathrm{n} = \nu_\mathrm{t} = 0.1$ normal and tangential relative damping coefficients and $\mu_\mathrm{t} = 0.305$ tangential friction coefficient.

Consequently, the parameters for the *particle-tool interaction* (and *particle-wall interaction*) have been set to $E_\mathrm{n} = 1.0 \cdot 10^9\,\frac{\mathrm{N}}{\mathrm{m}^2}$ and $E_\mathrm{t} = 1.2 \cdot 10^9\,\frac{\mathrm{N}}{\mathrm{m}^2}$ normal and tangential stiffness, $\nu_\mathrm{n} = \nu_\mathrm{t} = 0.1$ normal and tangential relative damping coefficients and $\mu_\mathrm{t} = 0.26$ tangential friction coefficient.

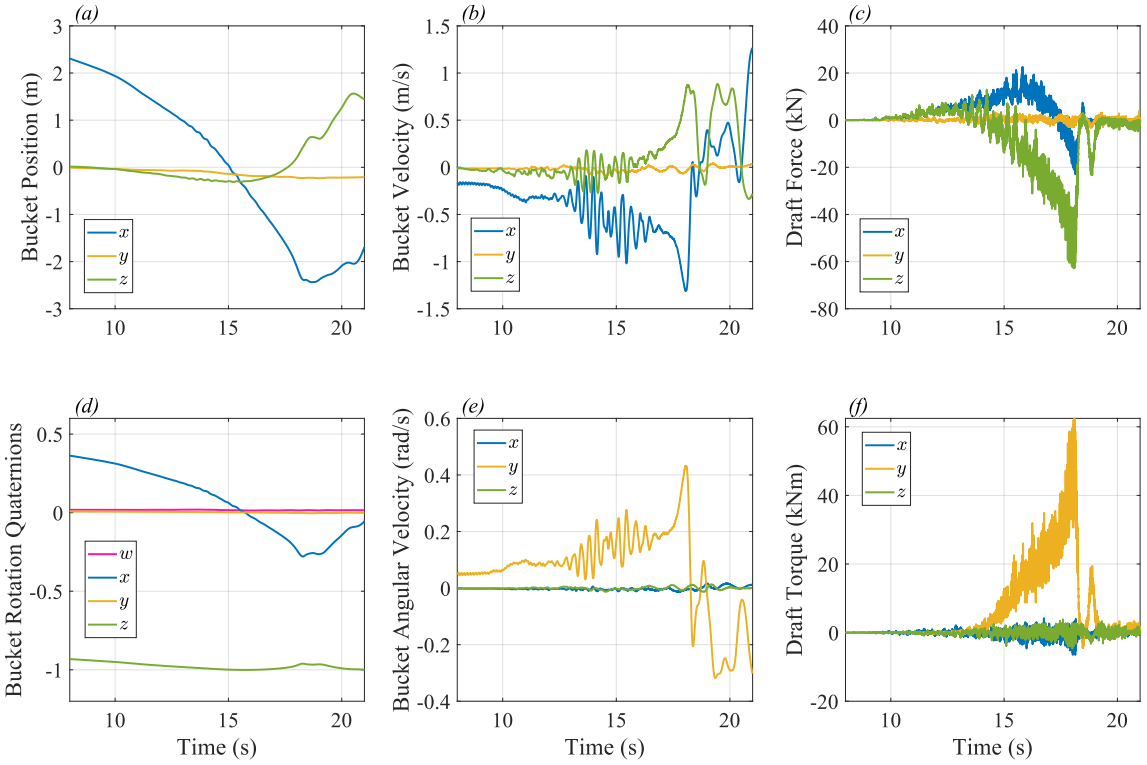

Figure 6. Co-simulation result of digging maneuver: Input telemetry of bucket position *(a)* and rotation (quaternions) *(d)*, translational *(b)* and rotational *(e)* velocity to the particle code and associated draft forces *(c)* and torques *(f)* in the particle simulation.

The material parameters for density have been set to $\rho_{\text{tool}} = 1000.0\,\frac{\text{kg}}{\text{m}^3}$ for wall and tool and to $\rho_{\text{soil}} = 2650.0\,\frac{\text{kg}}{\text{m}^3}$ for the granular soil. Following the sieving curve for the experimental soil sample, the grain size distribution has been set to a mean particle size $\mu = 0.040\,\text{m}$ and a standard deviation of $\sigma = 0.012\,\text{m}$, with minimum and maximum particle sizes of $d_{\text{min}} = 0.016\,\text{m}$ and $d_{\text{max}} = 0.063\,\text{m}$.

The particles have been dropped into the box from a generator box placed above, with an insertion frequency of $\nu = 4\,\text{Hz}$ and a mass flow rate of $\dot{m} = 16\,400\,\frac{\text{kg}}{\text{s}}$. The final test bed has a little less than $N = 1\,000\,000$ particles. A snapshot of the particle positions from this generation process has been saved and is loaded to the simulation framework before the co-simulation is started.

4.2 MBD-DEM Co-Simulation

During the co-simulation, the DEM solver is called from the Simulink-based MBD model via an FMU. This enables the user to start simulations from the Simulink environment without the need to switch between several interfaces during runtime. The FMU block contains the particle model parametrization as specified above in Section 4.1.2 and, additionally, the loaded particle position snapshot as well as the triangulated tool geometry, i.e., the bucket. Figure 5 shows snapshots of the maneuver during the co-simulation process.

Figure 6 shows the time series of the exchanged quantitites between the MBD and DEM solver. The bucket position (Figure 6*(a),(b),(d),(e)*) is moved in positive x-direction with a cutting depth of $0.30\,\text{m}$. The calculated feedback (Figure 6*(c),(f)*) is a resistive force in x- and z-direction at the beginning of the trajectory, with the force in z-direction changing sign when the bucket starts filling. The whole maneuver has been performed in the x-z-plane, thus the force component in y-direction and torque components in x- and z-direction don't have any notable contribution. The predicted draft force time series are in line to similar force curves obtained in earlier studies.

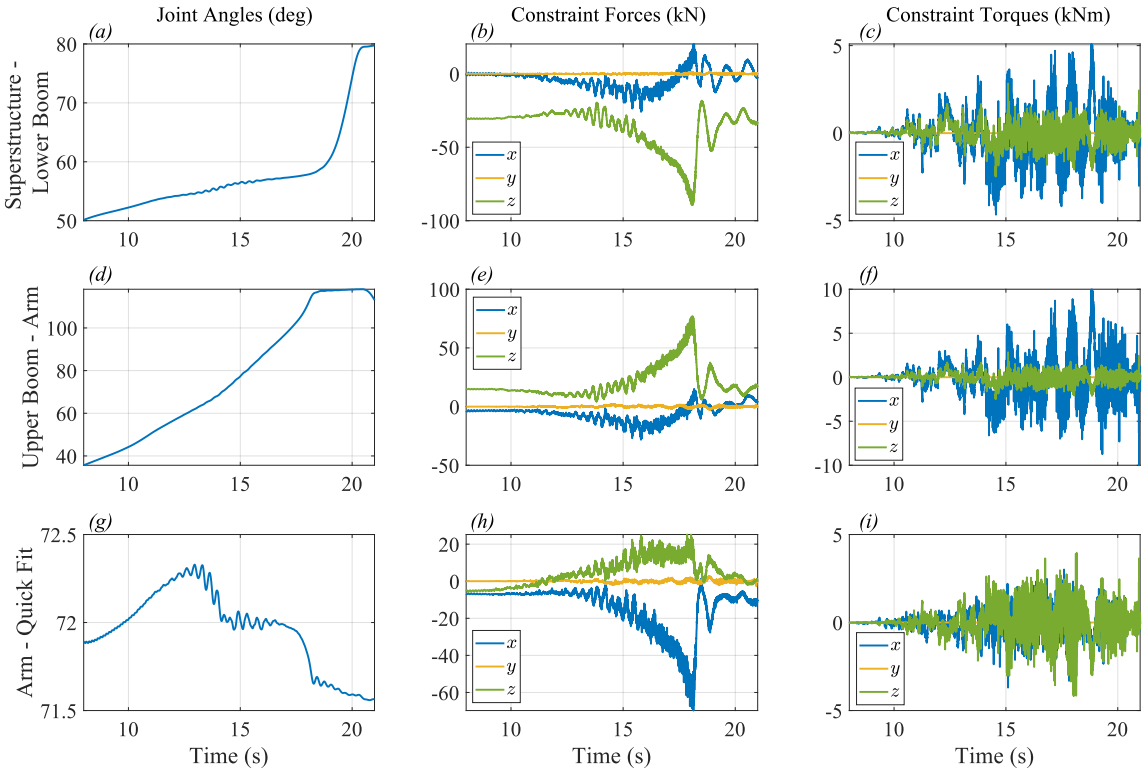

Figure 7. Time series of constraint forces in MBD model. *Left column:* Joint angles for the joints superstructure–lower boom *(a)*, upper boom–arm *(d)* and arm–quick fit *(g)* in local coordinates. *Center column:* Constraint forces for the joints superstructure–lower boom *(b)*, upper boom–arm *(e)* and arm–quick fit *(h)* in local base frame coordinates. *Right column:* Constraint torques for the joints superstructure–lower boom *(c)*, upper boom–arm *(f)* and arm–quick fit *(i)* in local base frame coordinates.

In contrast to a pure stand-alone simulation of a tool moving through a particle bed, the MBD-DEM co-simulation enables to access constraint forces of the joints between rigid bodies of the MBD model. Such forces enable the development engineer to access crucial quantities for the estimation of fatigue and durability properties of the simulated machine. In Figure 7, the constraint force and torque time series for the three main boom assembly joints of the excavator have been plotted together with the respective joint angle. Figure 5 can be consulted to clarify the allocation of the joints within in boom assembly. Starting from the excavator's main body, the first main joint connects the superstructure with the lower boom. The corresponding joint angle can be seen in Figure 7*(a)*, the constraint force and torque time series in panels *(b)* and *(c)*, respectively. Moving further through the boom assembly, the next main joint is connecting the upper boom with the arm. The joint angle is plotted in panel *(d)* with its corresponding force and torque time series in panels *(e)* and *(f)*. Consequently, panel *(g)* shows the joint angle for the last main joint, connecting the arm with the quick fit, which again connects to the tool itself. The corresponding force and torque time series are plotted in panels *(h)* and *(i)*.

As all three joints in question are one degree-of-freedom revolute joints around the local y-axis, there is no constraint torque in y-direction. The forces have been measured in local base frame coordinates, which are right-handed coordinate systems with the x-axis pointing backwards with respect to the operator view, and the z-axis pointing upwards. As the main movement takes place in the x-z-plane, it can be stated that the constraint force in y-direction and torques in x- and z-direction only play a minor role and can be neglected in the further discussion in this specific case. During the digging maneuver, the local arm coordinate system, being the base coordinate system for the constraint forces and torques acquired at the joint connecting arm and quick fit, is rotating by almost $180°$. Therefore, the constraint force in x-direction is taking the main

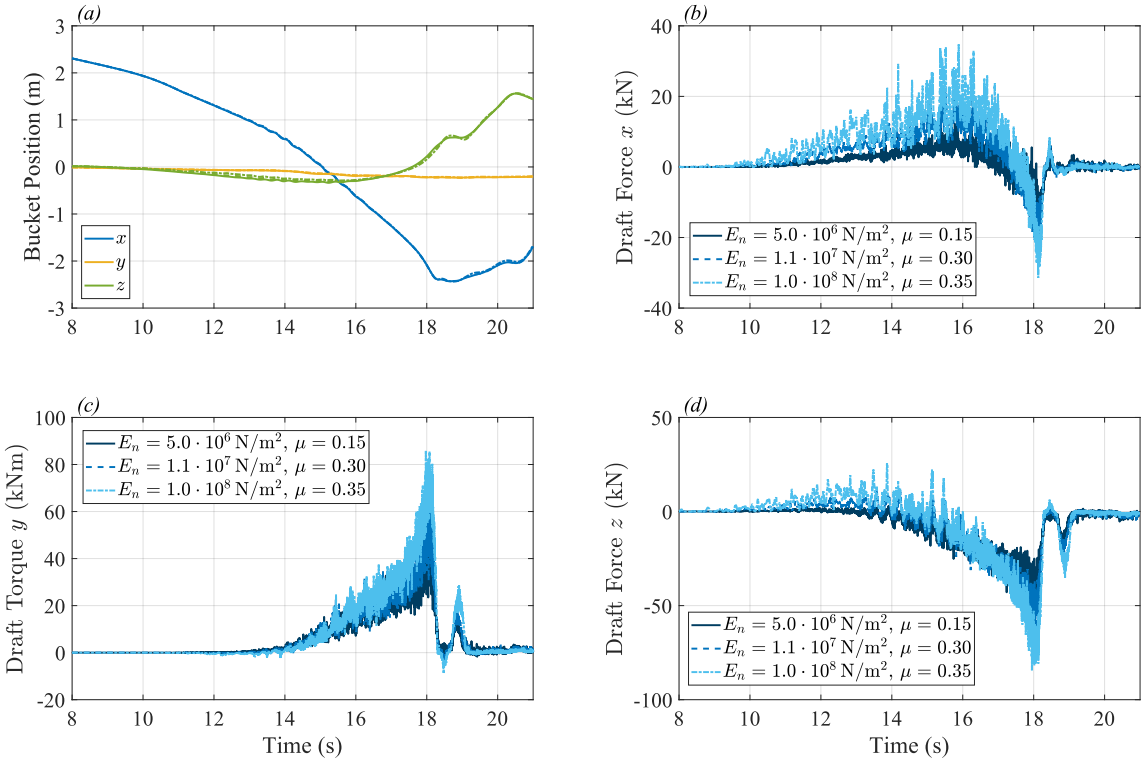

Figure 8. Variation of Particle Contact Parameters. Bucket trajectory data in x-, y- and z-direction for the three parameter sets *(a)*. Draft force in x-direction *(b)*, z-direction *(d)* and torque in y-direction *(c)* for the three parameter sets specified in the legend.

load of the particles collected by the bucket. This rotation is also the reason for the force in z-direction to stay positive during the whole maneuver, the z-axis is pointing downwards towards the end.

4.3 Influence of soil parametrization on draft forces

To close the loop to the soil characterization in Section 3 and underline the importance of a validated particle parametrization, especially in the context of DEM-MBD co-simulation, an exemplary parameter variation study has been executed. For this purpose, besides the parameter set resulting from the characterization in Section 3.5, parameter sets for a softer and a harder soil have been created artificially. Details of the three parameter sets used in the study are shown in Table 2. The tool trajectory and the MBD model have not been touched for the study, only the soil parametrization has been varied.

Table 2. Definition of the parameter sets as used for the executed parameter variation study. The parameter set called "medium soil" here corresponds to the result of Section 3.5.

Soil Type	E_n(N/m^2)	E_t(N/m^2)	ν_n	ν_t	μ
Soft Soil	$5.000 \cdot 10^6$	$6.00 \cdot 10^6$	0.1	0.1	0.150
Medium Soil	$1.125 \cdot 10^7$	$1.35 \cdot 10^7$	0.1	0.1	0.305
Hard Soil	$1.000 \cdot 10^8$	$1.20 \cdot 10^8$	0.1	0.1	0.350

The bucket trajectory is shown in Figure 8*(a)* for all three parameter sets. There are only minor variations in the cutting depths, resulting from the lower penetration resistance of softer soils.

For the resulting draft forces however, shown in Figure 8*(b),(c),(d)*, the soil parametrization has a notable influence. As has been identified in Section 4, the coordinates mostly involved in the digging maneuver

are the force in x- and z-direction and the torque in y-direction. For this reason, all other force and torque components have been omitted here.

Comparing the force and torque time series for the three soil parametrizations, it can clearly be seen that the absolute value is growing with harder soil parametrization, while the shape of the curves stays similar. The change in amplitude, which has already been observed in the context of a blade drawn through a particle bed [10], is especially critical, as it has a large influence on the constraint forces which are used in load data analysis to predict durability and fatigue properties of the machine parts under development.

Comparing the span within the different parameter sets used for this study with the sensitivity obtained during the virtual triaxial test, as shown in, e.g., Figure 2*(a)* for Young's modulus, it can be stated that the corresponding deviations in the predicted forces for the digging maneuver are smaller. In other words, this means that, at least for the presented maneuver, the requirement of a validated soil seem to be less strict than promoted in the introduction. However, there might be different maneuvers as, e.g., compaction, where the stress-strain behavior of a soil needs to be determined with even more precision. Finally, the observation shows the robustness of the presented workflow, as the method used for the optimization and validation is more sensitive on parameter variations than the actual application.

5 CONCLUSION

Within this article, the authors present a workflow for the generation of a validated particle model and apply it to the use case of the soil-tool interaction force prediction in the development of off-road machinery and vehicles. The prediction quality has been addressed by a dedicated calibration routine for the particle simulation model, resulting in a virtual soil sample that behaves similar to its real-world equivalent. The parametrization procedure has been executed, stressing the example of a gravel sand specimen, where validation is achieved by minimizing the deviations between the stress-strain curves obtained by a virtual and a real-world ISO triaxial test setup. The validated virtual gravel sand model has then been applied to a MBD-DEM co-simulation framework. There, it has been used to predict the draft forces acting on a wheeled excavator during a digging maneuver. This exemplary maneuver has been employed for a soil parameter variation study, showing the effects of parametrization on quality of the draft force prediction. The article shows the great potential of DEM-based particle simulation for industrial applications in the field of the development of heavy machinery and vehicles.

REFERENCES

[1] Bui, H. H.; Nguyen, G. D.: Smoothed Particle Hydrodynamics (SPH) and its Applications in Geomechanics: From Solid Fracture to Granular Behavior and Multiphase Flows in Porous Media. Comput Geotech, Vol. 138, 104315, 2021.

[2] Jing, L.: A review of Techniques, Advances and Outstanding Issues in Numerical Modelling for Rock Mechanics and Rock Engineering. Int J Rock Mech Min, Vol. 40, pp. 283–353, 2003.

[3] Cundall, P.; Strack, O.: A Discrete Numerical Model for Granular Assemblies. Geotechnique, Vol. 29, pp. 47–65, 1979.

[4] Coetzee, C. J.; Els, D. N. J.: The Numerical Modelling of Excavator Bucket Filling Using DEM. J Terramechanics, Vol. 46, pp. 217–227, 2009.

[5] Nezami, E. G.; Hashash, Y. M. A.; Zhao, D.; Ghaboussi, J.: Simulation of Front End Loader Bucket-Soil Interaction Using Discrete Element Method. Int J Numer Anal Met, Vol. 31, pp. 1147–1162, 2007.

[6] Shmulevich, I.; Asaf, Z.; Rubinstein, D.: Interaction Between Soil and a Wide Cutting Blade Using the Discrete Element Method. Soil Till Res, Vol. 97, pp. 37–50, 2007.

[7] Balzer, M.; Burger, M.; Däuwel, T.; Ekevid, T.; Steidel, S.; Weber, D.: Coupling DEM Particles to MBS Wheel Loader via Co-Simulation. In Berns, K.; Dressler, K.; Fleischmann, P.; Ilsen, R. Jörg,

B.; Kalmar, R.; Nagel, T.; Schindler, C.; Stephan, N. K. (eds) Proc. Commercial Vehicle Technology, pp. 479–490, Shaker Verlag, Aachen, 2016.

[8] Obermayr, M.; Dressler, K.; Vrettos, C.; Eberhard, P.: Prediction of draft forces in cohesionless soil with the Discrete Element Method. J Terramechanics, Vol. 48, pp. 347–358, 2011.

[9] Obermayr, M.: Prediction of Load Data for Construction Equipment using the Discrete Element Method. Dissertation, Universität Stuttgart, 2013.

[10] Jahnke, J.; Steidel, S.; Burger, M.; Jareteg, K.; Quist, J.: Efficient and Robust Parameter Identification for Soil modeled via the Discrete Element Method. In Berns, K.; Dressler, K.; Kalmar, R.; Stephan, N.; Teutsch, R.; Thul, M. (eds) Proc. Commercial Vehicle Technology, pp. 52–63, Springer Vieweg, Wiesbaden, 2022.

[11] Jahnke, J.; Steidel, S.; Burger, M.; Simeon, B.: Efficient Particle Simulation using a two-phase DEM-lookup approach. Proc. ECCOMAS on Multibody Dynamics, pp. 425–432, 2019.

[12] Jahnke, J.; Steidel, S.; Burger, M.; Papamichael, S.; Becker, A.; Vrettos, C.: Parameter Identification for Soil Simulation based on the Discrete Element Method and Application to Small Scale Shallow Penetration Tests. Proc. PARTICLES 2019, pp. 332–342, 2019.

[13] DIN EN ISO 17892-8:2018-07: Geotechnical Investigation and Testing - Laboratory Testing of Soil - Part 8: Unconsolidated Undrained Triaxial Test (ISO 17892-8:2018), German Version EN ISO 17892-8:2018.

[14] https://www.mathworks.com/products/simulink.html, last accessed April 04, 2024.

[15] https://fmi-standard.org/, last accessed April 04, 2024.

[16] Bilock, A.: A GPU Polyhedral Discrete Element Method. Master's thesis. Chalmers University of Technology, 2020.

[17] Quist, J. et al.: Investigation of the effect of size segregation on roller compaction of unbound materials. Technical report. Fraunhofer-Chalmers Centre for Industrial Mathematics, Computational Engineering & Design. Gothenburg, 2021.

[18] Sagar, V. R.; Lorin, S.; Göhl, J.; Quist, J.; Jareteg, K.; Cromvik, C.; Mark, A.; Edelvik, F.; Wärmefjord, K.; Söderberg, R.: A Simulation study on the effect of particle size distribution on the printed geometry in selective laser melting. Journal of Manufacturing Science and Engineering, 144(5), 051006, 2022.

[19] Eriksson, A. et al.: Numerical and Analytical Evaluation of Load Distribution Patterns on Ballasted Concrete Railway Bridges. In: Building for the Future: Durable, Sustainable, Resilient: Proceedings of the fib Symposium 2023-Volume 2. Springer Nature Switzerland, pp. 109–118, 2023. doi: 10.1007/978-3-031-32511-3_12.

[20] INTO-CPS Association: PyFMU. (2020) [Online]. Available: https://pypi.org/project/pyfmu/, Accessed on: April 5, 2024.

[21] Weinhart, T.; Hartkamp, R.; Thornton, A. R.; Luding, S.: Coarse-grained local and objective continuum description of three-dimensional granular flows down an inclined surface. Physics of Fluids 25, 070605, 2013.